Surface Micromachined Viscous Spiral Pump

M. I. Kilani*, P. C. Galambos**, Y. Haik*** and C-J. Chen***

*University of Jordan, Department of Mechanical Engineering
Amman, Jordan, kilani@eng.fsu.edu
**Sandia National Lab, pcgalam@sandia.gov
***Florida State University, haik@eng.fsu.edu and cjchen@eng.fsu.edu
2525 Pottsdamer St, Tallahassee, FL 32310

ABSTRACT

One distinguishing feature of micro scale fluid flow is its low Reynolds number, which is attributed to the small characteristic dimension and dominant viscous effects. Motivated by the observation that low Reynolds pumping on the macro-scale is often achieved by viscous drag, a micro-scale viscous drag pump, which drags fluid along a spiral-shaped channel, is developed using surface micromachining. The paper presents the detailed design of the mechanical elements of the pump and an analysis of the flow field in its spiral channel.

Keywords: micropump, surface micromachining, spiral, viscous.

1 INTRODUCTION

Several recent investigations discuss using viscous drag as the operating principle in micromachined pumps. The feasibility of this concept in the viscosity dominated microscale flow fields has been experimentally demonstrated using a rotating cylinder placed eccentrically between two parallel plates [1], and a number of analytical and numerical simulations have followed [2,3]. This paper introduces a new viscous drag micropump design that takes advantage of the shallow channel depths produced in surface micromachining, and addresses the planar nature by which this technology is limited. The design works by rotating a disk with a spiral protrusion at a close proximity over a stationary plate. The spiral protrusion produces the effect of the long channel described in Couette experiment, and the rotating disk assumes the role of the moving plate. For the purpose of analyzing the flow field in the pump, the spiral channel is approximated as a straight channel with a stationary bottom boundary and moving top and side boundaries. Analytical solution is obtained by based on the lubrication equations.

2 DESIGN

A schematic illustration of the viscous-type spiral pump concept is shown in Figure 1. A disk with a spiral protrusion rotates at a close proximity over a stationary plate and fluid is contained in the spiral channel created by the spiral protrusion and is bounded by the stationary plate on the bottom and by the rotating disk on the top. Due to non-slip conditions a velocity profile develops in the channel with fluid velocity increasing from zero at the stationary plate to the rotating plate velocity at the top. Viscous stresses on the upper and lower surfaces of the channel generate a pressure gradient along the channel and allow the fluid to be transported against an imposed pressure difference. Two holes at either end of the spiral channel provide the required inlet and outlet for the pumped fluid.

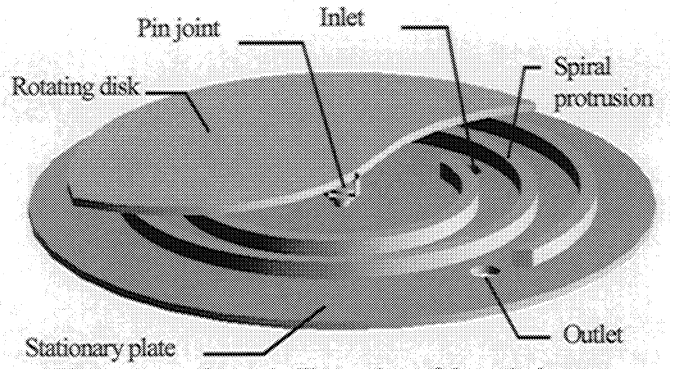

Figure 1. A schematic illustration of the spiral pump

Figure 2 shows an example viscous-type spiral micropump fabricated in SUMMiT technology and illustrates the power source and actuation mechanism used to rotate the spiral disk. A comb drive microengine provides continuous rotational motion on its pinion gear and mechanical power is transmitted to the spiral disk through a 12:1 torque amplification gear train. Both the microengine and the miorotransmission are available as pick and place components in SUMMiT design library [4].

The diameter of the pumping chamber enclosing the spiral disk in the design of figure 2 is 1200 microns and the width of the spiral wall is 21 microns. The distance between the upper disk and the stationary plate defines the height of the spiral channel and is equal to 10 microns. The centerline curve of the spiral channel is a linear Archimedean spiral described in polar coordinates by $r = k\theta + r_o$, $0 \le \theta \le \Delta\theta$. The values of the parameter k, r_o and $\Delta\theta$ is listed in Table 1 along with the spiral wall width w_t and the spiral channel height h. These five

parameters completely geometry define the spiral channel geometry.

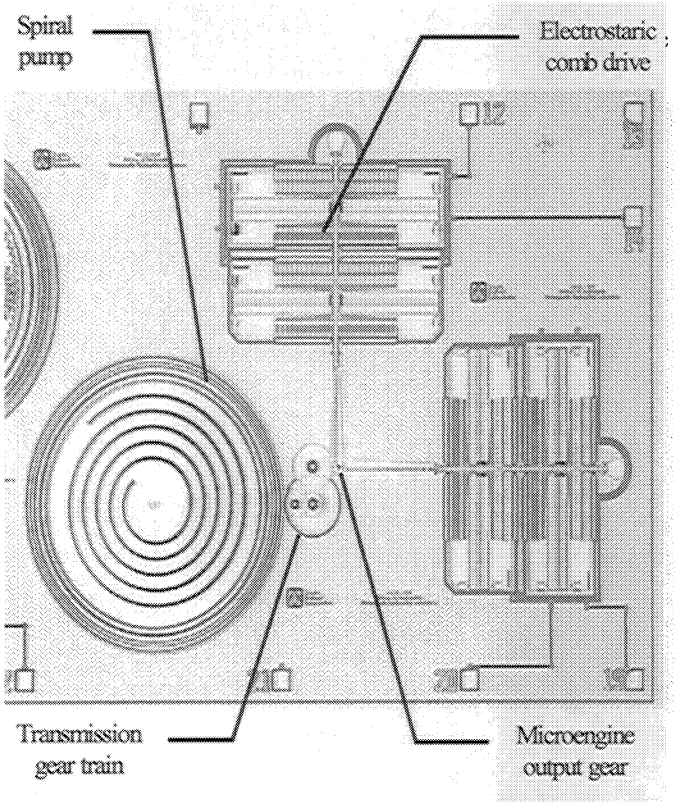

Figure 2. An example spiral micropump fabricated in SUMMiT

Parameter	Value
Polar slope k	12 microns
Starting radius r_o	146 microns
Angular span $\Delta\theta$	8π
Wall thickness w_t	21 microns
Channel height h	10 microns

Table-1 Spiral channel parameters for the design of figure 1 and figure 2.

Note that $k / r_o << 1$ indicating that the channel has a slight curvature at the entry and along its entire length. This condition is important for the viscous drag effect because it indicates that the rotation of the spiral causes the fluid to be dragged axially along the spiral channel and not normal to the channel.

3. SUMMiT IMPLEMENTATION

The spiral pump of figure 2 was fabricated in five levels of polysilicon using Sandia's Ultraplanar Multilevel MEMS Technology SUMMiT [5,6,7]. SUMMiT has the general features of a standard surface micro-machining process, including the deposition and lithographic patterning of alternate layers of polysilicon as the structural material, and silicon dioxide as the sacrificial material. The latest version provides five independent levels of low-stress polysilicon and offers chemical-mechanical planarization to eliminate inter-level interference. The bottom level labeled POLY0 serves as a ground level and the levels above, labeled POLY1 through POLY4 in that order are structural levels. The four intervening sacrificial oxide levels are labeled SOX1 through SOX4 with SOX1 standing between POLY0 and POLY1, SOX2 between POLY1 and POLY2 and so forth. Patterns through each SOX level allow the formation of anchors between the two surrounding POLY levels. SUMMiT provides a timed etch for SOX1, SOX3 and SOX4 levels to create dimples in POLY1, POLY3 and POLY4. The timed etch masks are labeled DIMPLE1, DIMPLE3 and DIMPLE4. Additionally, SUMMiT provides an isotropic etching step that targets SOX1 after depositing and patterning POLY1. This allows creating annular undercuts below POLY1, which when followed by a conformal deposition of SOX2 and POLY2 create the effect of a revolute joint between POLY1 and POLY2.

Figure 3 shows a cross sectional view through the centerline of the rotating spiral disk to illustrate the interconnections between the different polysilicon levels in the design produced. The rotating disk is defined in the upper polysilicon level POLY4 and the stationary plate in the ground level POLY0. The spiral protrusion is defined in POLY1, POLY2 and POLY3 and is anchored to the POLY4 rotating disk. Dimples in the POLY1 level are defined below the spiral wall leaving only a small gap between the spiral and the stationary POLY0 level. A pin joint at the center of the disk provides rotational freedom. Gear teeth on the perimeter of the disk mesh with matching teeth on the output gear of the transmission gear train and provide continuous rotation. The inlet and outlet holes are created through backside of the wafer using a Bosch etching process [8].

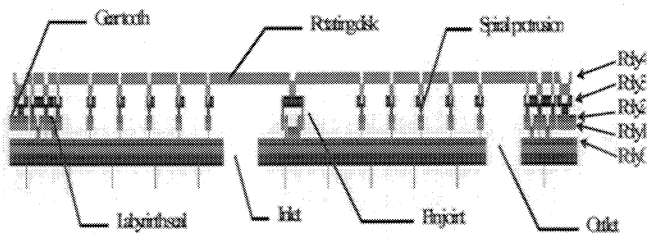

Figure 3. A cross section through the spiral disk centerline (Vertical dimension magnified to show details)

A labyrinth sealing approach was employed to prevent the pumped fluid from leaking outside the pumping chamber. This approach is based on enclosing the pumping

chamber by three concentric cylindrical shells that stand between the rotating disk and the fixed plate. The inner and outer shells are attached to the stationary plate while the middle shells is attached to the rotating disk with a small clearance allowed between the shells. A close-up view of the labyrinth seal of figure 3 is shown in figure 4. The three shells are defined in POLY1, POLY2 and POLY3 levels. The middle shell is attached to the rotating disk in POLY4 while the inner and outer shells attached to the POLY0 ground.

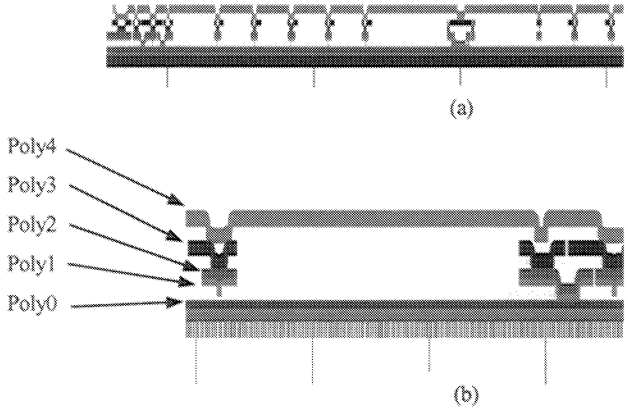

Figure 4. Labyrinth seal

The mask layout used to produce the labyrinth seal is detailed in figure 5. Part (a) shows the complete layer layout and illustrates the meshing between gear teeth on the spiral disk and the matching teeth on the output of the transmission train. Part (b) shows the nitride cut mask which produce the outlet port in Bosch etching. Part (c) shows the POLY0 ground level defined under the entire moving parts in the mechanism. SOX1 cuts anchor the inner and the outer labyrinth shells to POLY0. DIMPLE1 cuts under the spiral channel and under the middle labyrinth wall improve the sealing between the flights of the spiral channel and that of the labyrinth seal. The meshing between the gears of the spiral disk and the output gear of the transmission takes place in POLY2.

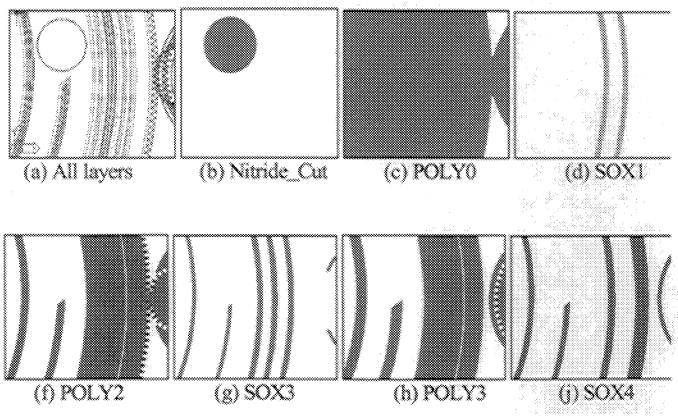

Figure 5. Mask layouts for the labyrinth seal

4. FLUID MODELING

For the purpose of analyzing the flow field in the spiral channel we shall neglect the curvature of the spiral and replace it with a straight channel of the same dimensions and boundary conditions. This assumption is valid when $k/r << 1$. Given a spiral channel with height h, wall thickness w_t, and centerline segment defined by $r = k\theta + r_o,\ 0 \le \theta \le \Delta\theta$,

and satisfying conditions $k/r_o << 1$

.If the channel is rotating at an angular velocity ω against a pressure difference Δp, the flow field in the channel may be modeled by a straight model with the mapping relations listed in Table 2.

Parameter	Relation
Straight channel width	$2\pi k - w_t$
Straight channel length	$(r_o + k\Delta\theta/2)\Delta\theta = r_a\Delta\theta$
Straight channel height	h
Axial velocity	$u_{ch}(x) = \omega r_o + k\omega x / r_a$
Transverse velocity	0
Pressure difference	Δp

Table 2. Mapping a spiral channel geometry into a straight channel representation

Because both the geometry and boundary conditions of the straight channel model are symmetric around the plane $z = 0$ and since $h << w$ in the shallow channels of surface micromachined devices, the flow field along the channel may be represented by the flow in the plane of symmetry, which reduces the flow model into to the 2D model of figure 6

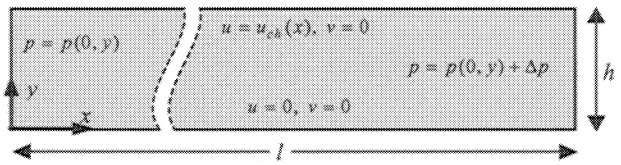

Figure 6. The accelerated Couette model

5. ANALYSIS

The microscale flow field of an incompressible Newtonian fluid the in thin narrow gap of the model depicted in figure 7 is a classical example of flow situation governed by the simplified version of the Navier-Stokes equations known as the lubrication equations [10]. Taking the x axis along the channel axis and letting u and v denote the x and y components of the fluid velocity, p fluid pressure and μ its viscosity, the lubrication equations are

$$\frac{\partial p}{\partial x} = \mu \frac{\partial^2 u}{\partial y^2},\ \frac{\partial p}{\partial y} = 0 \qquad (1)$$

$$\frac{\partial u}{\partial x}+\frac{\partial v}{\partial y}=0 \qquad (2)$$

Equation (1) is the momentum conservation in the x and y direction while (2) is the continuity equation. In the case of figure 6, these equations are subject to the following boundary conditions

$$u(x,0)=0,\ u(x,h)=u_{ch}(x) \qquad (3)$$

$$v(x,0)=0,\ v(x,h)=0 \qquad (4)$$

$$p(l,y)=p(0,y)+\Delta p \qquad (5)$$

Equations (3) and (4) are the non-slip conditions on upper and lower walls of the channel and equation (5) is a consequence of imposing an external pressure Δp on the flow. This is the pressure head the pump needs to work against.

The lubrication equations are a linear set of equations and an analytical solution for the boundary conditions specified may be obtained by eliminating p from (1) to give $\frac{\partial^3 u}{\partial y^3}=0$ which by repeated integration leads to

The lubrication equation leads to an analytical solutions for the velocity components u and v

Defining the boundary velocity's deviation from the mean $\delta(x)$ as

$$\delta(x)=u_{ch}(x)-\overline{u}_{ch}$$

Table 3 summarizes the field and performance relations for the accelerated Couette model. As expected, when $\delta(x)=0$ along the channel these relations reduce to the corresponding relations obtained in Couette experiment with an upper plate velocity equal to the mean channel velocity

Quantity	Formula
Vertical velocity	$v=h\delta'(x)\left((y/h)^2-(y/h)^3\right)$
Axial velocity	$u=u_{ch}(x)\frac{y}{h}-\left(\frac{h^2\Delta p}{2\mu l}+3\delta(x)\right)\left(\frac{y}{h}-(\frac{y}{h})^2\right)$
Pressure	$p=\Delta p\frac{x}{l}+p_o+\frac{\mu}{h^2}\left(6\int_0^{x^*}\delta(x)dx-\delta'(x)(3y^2-2yh)\right)$
Volume flow rate	$q=\frac{h\overline{u}_{ch}}{2}-\frac{h^3}{12\mu l}\Delta p$
Force on moving	$F=\frac{\mu l\overline{u}_{ch}}{h}+\frac{h\Delta p}{2}$
Power	$P=\frac{\mu l\overline{u}_{ch}^2}{h}+\frac{h\Delta p\overline{u}_{ch}}{2}+4\frac{\mu}{h}\int_0^l\delta^2(x)dx$

Table 3 Summary of performance relations

To establish a sense of the expected performance figures of an actual spiral micropumps design, consider the case of pumping water ($\mu=1\times10^{-3}$ kg/(m.s)) using a spiral pump with the design parameters listed in table 1. Table 4 lists the theoretical flow rate, torque and power from the pump and the magnitude of these quantities for $\omega=1000$ rad/s (9550 rpm) when $\Delta p=0$ and $\Delta p=100$ Kpa.

	Performance relation	$\Delta p=($	$\Delta p=100$ K
Q (nanoliters per second)	$Q=81\times10^{-3}\omega-610\times10^{-}$	81	20
T (nano N.m)	$T=3.57\times10^{-3}\omega+80.7\times1$	3.57	11.64
P (micro Watts)	$P=4.80\times10^{-3}\omega^2+80.7\times$	4.80	12.87

Table 4 Flow rate, torque and power

REFERENCES

1. SEN, M., WAJERSKI, D., & GAD-ELHAK, M. 1996 A novel pump for MEMS Applications. *Trans. ASME: J. Fluid Engng* **118**, 624-627
2. SHARACHANDRA, M. C., SEN, M.& GAD-ELHAK, M. 1997 Navier-Stokes simulations of a novel viscous pump. *Trans. ASME: J. Fluid Engng* **119**, 372-382
SMITH, J. 1996 Micromachined sensor and actuator research at Sandia's Microelectronics Development Laboratory. *Proc. Sensors Expo* Anaheim '96, pp. 119-123
3. DAY, R. & STONE H. 2000 Lubrication analysis and boundary integral simulations of a viscous micropump. *J Fluid Mech.* **416**, 197-216
4. GARCIA, E. & SNIEGOWSKI J. 1995 Surface micromachined microengines *Sensors and Actuators* **48**, 203-214
5. SNIEGOWSKI, J & DE BOER, M. 2000 IC-compatible polysilicon surface micromachining. *Annu. Rev. Mater. Sci.* **30**, 299-333
6. KILANI, M., GALAMBOS, P., HAIK Y. & CHEN, C.J. 2001 University - National laboratory collaboration on MEMS design education. *Proc. ASME International Mechanical Engineering Congress and Exposition,* NewYork, NY
7. BUSTILLO, J., HOWE, R. & MULLER R. 1998 Surface micromachining for microelectromechanical systems. *Proceedings of the IEEE*, **v 86, n 8** 1552-1573
8. BOSCH, 1996 Patent No. 5501893 Method of anisotropically etching silicon *Robert Bosch Gmblt*